J Solid State Electrochem (2012) 16:429–434
DOI 10.1007/s10008-011-1347-2

ORIGINAL PAPER

Electrochemical studies of $LiCr_xFe_xMn_{2-2x}O_4$ in an aqueous electrolyte

Wanmei Xu · Anbao Yuan · Yuqin Wang

Received: 23 October 2010 / Revised: 30 January 2011 / Accepted: 17 February 2011 / Published online: 6 April 2011
© Springer-Verlag 2011

Abstract In this paper, $LiCr_xFe_xMn_{2-2x}O_4$ (x=0, 0.05, 0.1) electrode materials were prepared by sol–gel technique and characterized by X-ray diffraction (XRD) and transmission electron microscopy or high-resolution transmission electron microscopy techniques. XRD results reveal that the Cr–Fe-co-doped $LiCr_xFe_xMn_{2-2x}O_4$ materials are phase-pure spinels. The electrochemical properties of the $LiMn_2O_4$, $LiCr_{0.05}Fe_{0.05}Mn_{1.9}O_4$, and $LiCr_{0.1}Fe_{0.1}Mn_{1.8}O_4$ electrodes in 5 M $LiNO_3$ aqueous electrolyte were investigated using cyclic voltammetry, AC impedance, and galvanostatic charge/discharge methods. In the current range of 0.5–2 A g^{-1}, the specific capacity of the $LiCr_{0.05}Fe_{0.05}Mn_{1.9}O_4$ electrode is close to that of the $LiMn_2O_4$ electrode, but the specific capacity of the $LiCr_{0.1}Fe_{0.1}Mn_{1.8}O_4$ electrode is obviously lower than that of the $LiMn_2O_4$ electrode. When the electrodes are charge/discharge-cycled at the high current rate of 2 A g^{-1}, the $LiCr_{0.05}Fe_{0.05}Mn_{1.9}O_4$ electrode exhibits an initial specific capacity close to that of the $LiMn_2O_4$ electrode, but its cycling stability is obviously prior to that of the $LiMn_2O_4$ electrode.

Keywords Spinel lithium manganese oxide · Chromium–iron substitution · Sol–gel · Electrochemical performance · Aqueous electrolyte

Introduction

Positive electrode material $LiMn_2O_4$ for Li-ion batteries has the merits of abundant manganese resources, low cost, facile preparation, and being eco-friendly. Compared with nonaqueous Li-ion batteries, aqueous Li-ion batteries have the advantages of good safety, low cost, and high ionic conductivity of the electrolyte. Spinel $LiMn_2O_4$ attracted great attentions as positive electrode material for aqueous Li-ion batteries [1–11]. Stoichiometric spinel $LiMn_2O_4$ takes the cubic framework by close-stacked O^{2-} ions at the 32e sites [12], which can be simply expressed as $[Li]_{8a}[Mn^{4+}Mn^{3+}]_{16d}[O_4]_{32e}$. When $LiMn_2O_4$ is discharged in the 3-V region, a structural transformation from cubic spinel phase to tetragonal rock-salt phase will happen, i.e., Jahn–Teller distortion, and result in poor cyclability. Several studies demonstrated that partial substitution of Al^{3+}, Co^{3+}, Cr^{3+}, Fe^{3+}, or Mg^{2+}, etc., for Mn^{3+} in $LiMn_2O_4$ can suppress the Jahn–Teller effect in a certain extent and hence can improve the cycling stability of $LiMn_2O_4$ in nonaqueous electrolytes [13–17]. Except for single metal doping, there are studies about bimetal doping, such as Co–Al, Co–Cr, Cr–Al, and Fe–Cr doping [18–20]. Up to the present, only few studies about cation-doped $LiMn_2O_4$ in aqueous electrolyte have been reported. Hwang et al. investigated the structure variation of the Al-doped $LiAl_{0.15}Mn_{1.85}O_4$ upon charge/discharge in an aqueous $LiNO_3$ solution by in situ X-ray diffraction (XRD) method [21]. Cvjeticanin et al. studied the cyclic voltammetric behaviors of the Cr-doped $LiCr_{0.15}Mn_{1.85}O_4$ electrode in an aqueous $LiNO_3$ solution [8]. Stojkovic et al. investigated the improvement of Li^+ insertion behavior of the Cr-doped $Li_{1.05}Cr_{0.10}Mn_{1.85}O_4$ with addition of vinylene carbonate to a $LiNO_3$ aqueous solution [22]. Recently, we reported the electrochemical performances of the Al-doped $LiAl_xMn_{2-x}O_4$ in an aqueous $LiNO_3$ solution with improved high-rate cyclability [23].

In the present work, the Cr–Fe-doped $LiCr_xFe_xMn_{2-2x}O_4$ (x=0, 0.05, 0.1) electrode materials were prepared by

W. Xu · A. Yuan (✉) · Y. Wang
Department of Chemistry, College of Sciences,
Shanghai University,
Shanghai 200444, People's Republic of China
e-mail: abyuan@shu.edu.cn

sol–gel route. The electrochemical performances of the $LiMn_2O_4$, $LiCr_{0.05}Fe_{0.05}Mn_{1.9}O_4$, and $LiCr_{0.1}Fe_{0.1}Mn_{1.8}O_4$ electrodes in 5 M $LiNO_3$ aqueous solution are investigated and compared.

Experimental

Preparation of $LiCr_xFe_xMn_{2-2x}O_4$ (x=0, 0.05, 0.1) materials

Stoichiometric amounts of lithium acetate ($CH_3COOLi\cdot 2H_2O$), chromium nitrate ($Cr(NO_3)_3\cdot 9H_2O$), ferric nitrate ($Fe(NO_3)_3\cdot 9H_2O$), and manganese acetate ($(CH_3COO)_2Mn\cdot 4H_2O$) were dissolved in distilled water. In addition, the required amount of citric acid ($C_6H_8O_7\cdot H_2O$, the molar ratio of citric acid to the total amount of metal ions is 1:1) was dissolved in distilled water. The two solutions were mixed and stirred with a magnetic stirrer. After stirring for about 10 min, a given amount of polyethylene glycol (PEG−200) was added dropwise to the solution (in favor of the gelation process afterwards and as a dispersant). Then, strong aqua ammonia was added to the solution drop by drop until pH≈7. The solution was heated to 80 °C and kept at this temperature for water evaporation under stirring. With continuous evaporation, the solution became a semi-transparent sol with purple color and, finally, a concentrated gel was obtained. The gel was dried in a drying box at 105 °C for 4 h and then was ground to fine powder (precursor). The precursor was calcined in air in a muffle furnace at 700 °C for 12 h. After cooling to room temperature, the $LiCr_xFe_xMn_{2-2x}O_4$ (x=0, 0.05, 0.1) materials were obtained.

Characterization of $LiCr_xFe_xMn_{2-2x}O_4$ materials

XRD analysis of the $LiCr_xFe_xMn_{2-2x}O_4$ materials was conducted on a Rigaku D/max-2000 X-ray powder diffractometer with a Cu K_α radiation (40 kV, 40 mA) over the 2θ range 10–90°. Morphological observation of the pristine $LiMn_2O_4$ material was carried out using a JEOL JEM-200CX transmission electron microscope (TEM). Morphological observation and elemental analysis of the Cr–Fe-doped $LiCr_xFe_xMn_{2-2x}O_4$ materials were carried out using a JEOL JEM-2010 F high-resolution transmission electron microscopy (HRTEM) with an Oxford INCA energy dispersion spectroscopy (EDS).

Fabrication and electrochemical testing of $LiCr_xFe_xMn_{2-2x}O_4$ electrodes

$LiCr_xFe_xMn_{2-2x}O_4$ electrodes were fabricated as follows: $LiCr_xFe_xMn_{2-2x}O_4$ active material, acetylene black (AB), conductor and polytetrafluoroethylene binder (PTFE emulsion) were mixed thoroughly to form slurry. The slurry was coated onto a titanium mesh current collector with an apparent area of 1×1 cm, dried at 80 °C for 12 h, and then roll-pressed to a sheet. The weight ratio $LiCr_xFe_xMn_{2-2x}O_4$/AB/PTFE is 75:20:5.

Electrochemical measurements of the $LiCr_xFe_xMn_{2-2x}O_4$ electrodes were performed in a three-electrode glass cell, with $LiCr_xFe_xMn_{2-2x}O_4$ and activated carbon as working and counter-electrodes, respectively, and saturated calomel electrode (SCE) as reference electrode and 5 M $LiNO_3$ aqueous solution as electrolyte. Cyclic voltammetry and AC impedance measurements were carried out using Solartron Instrument Model 1287 coupled with a 1255B FRA. Charge/discharge tests were conducted using a LAND 2001A autocycler (China). All of the tests were conducted at 30 °C.

Results and discussion

Structural analysis and morphological observation

Figure 1 shows the XRD patterns of the $LiMn_2O_4$, $LiCr_{0.05}Fe_{0.05}Mn_{1.9}O_4$, and $LiCr_{0.1}Fe_{0.1}Mn_{1.8}O_4$ materials. As can be seen, the three materials exhibit the characteristic diffraction peaks of the cubic spinel $LiMn_2O_4$ with *Fd*3*m* space group (PDF 35–0782). A weak diffraction peak can be observed at ca. 32.5° for the pristine $LiMn_2O_4$ material, which corresponds to the strongest characteristic diffraction peak of Mn_2O_3 (PDF 78–0390), indicating the presence of a trace amount of Mn_2O_3 impurity phase in this material, while the two doped materials do not show any impurity diffraction peak, suggesting the phase-pure spinel structure of the $LiCr_xFe_xMn_{2-2x}O_4$ materials. These results suggest that Cr–Fe doping can hinder the formation of Mn_2O_3 phase in the calcination process. Compared with the pristine

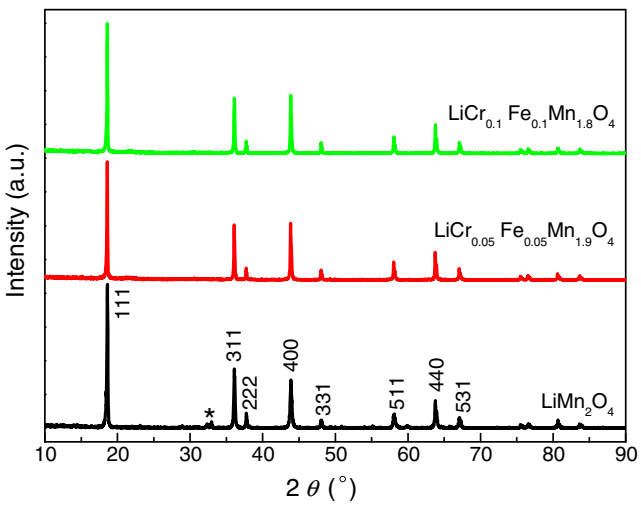

Fig. 1 XRD patterns of $LiCr_xFe_xMn_{2-2x}O_4$ (x=0, 0.05, 0.1) materials

$LiMn_2O_4$, the diffraction peaks of the $LiCr_xFe_xMn_{2-2x}O_4$ narrow down, and the diffraction peak intensity of the (400) plane is increased. The peak intensity ratios of the (400) plane to (311) plane, $I_{(400)}/I_{(311)}$, for the $LiMn_2O_4$, $LiCr_{0.05}Fe_{0.05}Mn_{1.9}O_4$, and $LiCr_{0.1}Fe_{0.1}Mn_{1.8}O_4$ are 0.815, 1.031 and 1.050, respectively, which are similar to the variation regularity of $I_{(400)}/I_{(311)}$ for the $LiCr_xMn_{2-x}O_4$ (x=0, 0.05, 0.1, 0.15) materials prepared by high-temperature solid reaction (HTSR) [24]. For the $LiFe_yMn_{2-y}O_4$ ($0\le y\le 1$) materials prepared by HTSR [25], when $0\le y\le 0.5$, the variation of $I_{(400)}/I_{(311)}$ has also the similar regularity, i.e., the ratio $I_{(400)}/I_{(311)}$ increases with increasing y. However, when the concentration of Fe is increased to $y\ge 0.7$, the ratio $I_{(400)}/I_{(311)}$ is per contra decreased. For another $LiFe_yMn_{2-y}O_4$ ($0\le y\le 1$) materials prepared by HTSR [26], when $0<y<0.6$, all the Fe^{3+} ions occupy the octahedral 16d sites; when $y>0.6$, the peak intensity of the (220) plane increases with increasing y. Particularly, when y=1.0, the peak intensity of the (220) plane and subsequently the ratio $I_{(220)}/I_{(311)}$ increase obviously, while the peak intensity of the (400) plane and the ratio $I_{(400)}/I_{(311)}$ decrease obviously. These suggest that the additional Fe^{3+} ions partially occupy the tetrahedral 8a sites, forming the intermediate structure of $Li_{1-z}Fe_z[Li_zFe_{y-z}Mn_{2-y}]O_4$ between normal spinel and anti-spinel. For the bimetal-doped $LiM_yCr_{0.5-y}Mn_{1.5}O_4$ (M = Fe or Al; $0.0\le y\le 0.4$) materials prepared by HTSR [20], the ratio $I_{(400)}/I_{(311)}$ decreases with increasing y, while the ratio $I_{(220)}/I_{(311)}$ increases with increasing y, suggesting that with an increase in the concentration of the substitution ions (Fe^{3+} or Al^{3+}) the extent of occupation of the substitution ions on the tetrahedral 8a site increases. In the present work, no diffraction peaks of (220) plane could be observed in the XRD spectra of the $LiCr_xFe_xMn_{2-x}O_4$ materials. Judging from the XRD spectra and the above discussion, the Cr and Fe in $LiCr_{0.05}Fe_{0.05}Mn_{1.9}O_4$ and in $LiCr_{0.1}Fe_{0.1}Mn_{1.8}O_4$ in the present work should replace the Mn in 16d site.

Figure 2a shows the TEM photograph of the pristine $LiMn_2O_4$ material, and Fig. 2b, c shows the HRTEM photographs of the $LiCr_{0.05}Fe_{0.05}Mn_{1.9}O_4$ and $LiCr_{0.1}Fe_{0.1}Mn_{1.8}O_4$ materials, respectively. As can be seen in Fig. 2a, the pristine $LiMn_2O_4$ material consists of aggregates of regular crystallites with a size of ca. 200 nm. As can be seen in Fig. 2b, c, the $LiCr_{0.05}Fe_{0.05}Mn_{1.9}O_4$ and $LiCr_{0.1}Fe_{0.1}Mn_{1.8}O_4$ materials consist of aggregates of regular crystallites with different crystallite sizes, ranging from ca. 150 to 200 nm for the majority of the $LiCr_{0.05}Fe_{0.05}Mn_{1.9}O_4$ crystallites and ca. 200 to 300 nm for the majority of the $LiCr_{0.1}Fe_{0.1}Mn_{1.8}O_4$ crystallites. EDS analysis results reveal that the molar ratio of Cr–Fe–Mn=0.06:0.06:1.88 for the $LiCr_{0.05}Fe_{0.05}Mn_{1.9}O_4$ material and Cr–Fe–Mn=0.09:0.10:1.81 for the $LiCr_{0.1}Fe_{0.1}Mn_{1.8}O_4$ material. These results are close to the designed compositions of the materials.

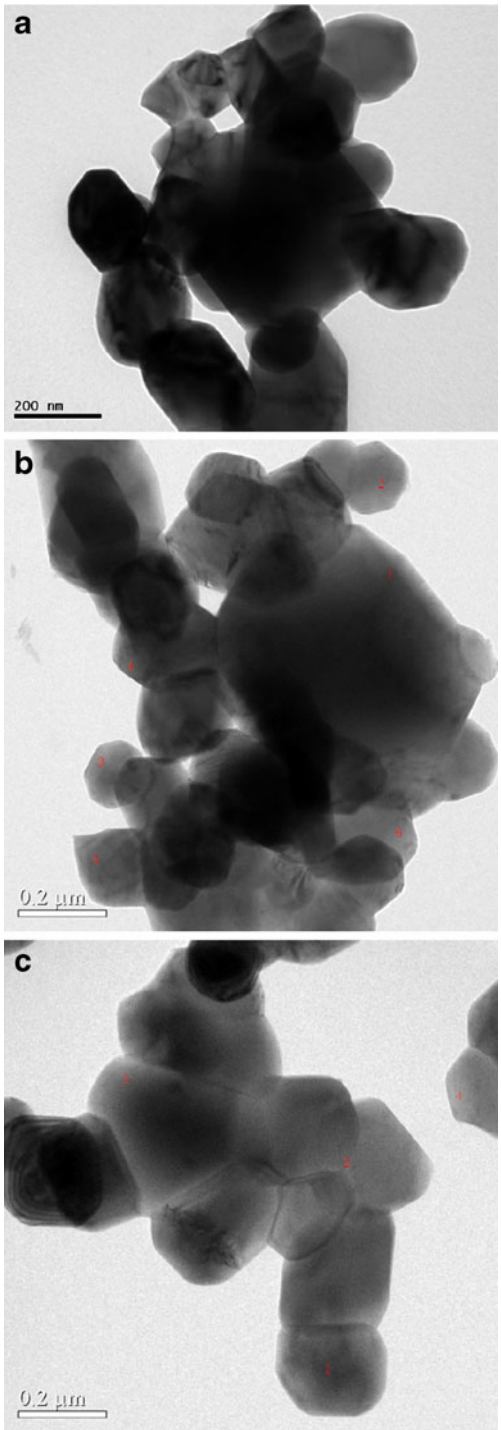

Fig. 2 TEM photograph of $LiMn_2O_4$ (**a**) and HRTEM photographs of $LiCr_{0.05}Fe_{0.05}Mn_{1.9}O_4$ (**b**) and $LiCr_{0.1}Fe_{0.1}Mn_{1.8}O_4$ (**c**)

Electrochemical performance

Figure 3 shows the cyclic voltammographs (CVs) of the $LiMn_2O_4$, $LiCr_{0.05}Fe_{0.05}Mn_{1.9}O_4$, and $LiCr_{0.1}Fe_{0.1}Mn_{1.8}O_4$ electrodes at a scan rate of 1 mV s^{-1}. The specific current data are obtained based on the weight of the $LiCr_xFe_x$

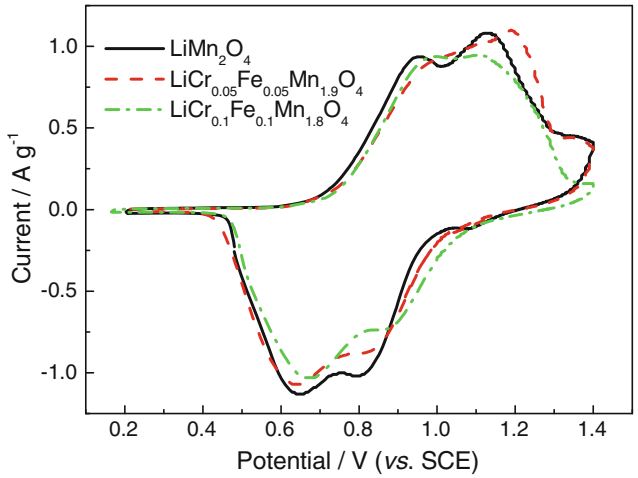

Fig. 3 Cyclic voltammographs of $LiCr_xFe_xMn_{2-2x}O_4$ (x=0, 0.05, 0.1) materials at a scan rate of 1 mV s^{-1}

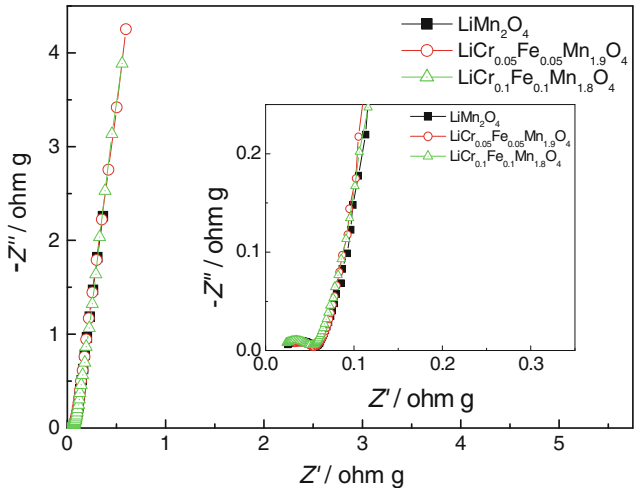

Fig. 4 Nyquist plots of $LiCr_xFe_xMn_{2-2x}O_4$ (x=0, 0.05, 0.1) electrodes

$Mn_{2-2x}O_4$ active materials. As can be seen, in the potential range of 0.2–1.4 V (SCE), the pristine $LiMn_2O_4$ electrode presents two clear couples of redox waves, which correspond to deintercalation and intercalation of Li^+ ions in $LiMn_2O_4$ [8]. Compared with the pristine $LiMn_2O_4$ electrode, the redox peak potentials of the $LiCr_{0.05}Fe_{0.05}Mn_{1.9}O_4$ electrode move toward a positive direction, and the reduction peak current is decreased, especially for the high-potential reduction peak current. The peak currents of the $LiCr_{0.1}Fe_{0.1}Mn_{1.8}O_4$ electrode are decreased obviously, especially for the high-potential redox peaks, and the reduction peak potentials move toward a positive direction. According to literatures [27, 28], in nonaqueous organic electrolyte, the redox peak currents of Cr- or Fe-doped $LiMn_2O_4$ electrode is decreased compared to that of a pristine $LiMn_2O_4$ electrode, especially for the high-potential redox peaks, and the peak potentials move toward a positive direction. Shi et al. investigated the effect of cations doping on the electron structure of the spinel $LiM_yMn_{2-y}O_4$ (M = Cr, Mn, Fe, Co and Ni) by first principles method [29]. Computational results demonstrated that a new M-3d band occurred in the density of states of doped $LiM_yMn_{2-y}O_4$ compared to $LiMn_2O_4$. Simultaneously, a corresponding new O-2p band appeared in the energy range around Fermi energy level due to the interaction between M-3d and O-2p. Thus, the new O-2p band at the low energy level will induce a higher intercalation potential because that removing electrons from low O-2p energy level needs more energy. Hence, the existence of a higher intercalation potential for the doped $LiM_yMn_{2-y}O_4$ should be ascribed to the low O-2p energy level induced by the cations doping.

Figure 4 shows the Nyquist plots of the $LiMn_2O_4$, $LiCr_{0.05}Fe_{0.05}Mn_{1.9}O_4$, and $LiCr_{0.1}Fe_{0.1}Mn_{1.8}O_4$ electrodes over the frequency range of 10^5–10^{-2} Hz, and the inset is the enlargement of the impedance in a high-frequency region. The impedance data are calculated based on the weight of the $LiCr_xFe_xMn_{2-2x}O_4$ active materials and normalized in Ohm grams. As can be seen, all the impedance plots consist of a high-frequency small arc and a low-frequency line. The high-frequency arc should be ascribed to the charge transfer process, reflecting the charge transfer resistance, and the low-frequency line corresponds to the solid diffusion of Li^+ ions in $LiCr_xFe_xMn_{2-2x}O_4$. No obvious difference could be observed between the three electrodes. In addition, the charge transfer resistance is small compared to the diffusion impedance, suggesting that the electrode reaction kinetics is governed by the solid diffusion process.

Figure 5a, b shows the discharge-specific capacities of the $LiMn_2O_4$, $LiCr_{0.05}Fe_{0.05}Mn_{1.9}O_4$, and $LiCr_{0.1}Fe_{0.1}Mn_{1.8}O_4$ electrodes at different charge/discharge current rates and the charge/discharge curves at the current rate of 0.5 A g^{-1}, respectively. The values of current rate and specific capacity are calculated based on the weight of the $LiCr_xFe_xMn_{2-2x}O_4$ active materials. As can be seen in Fig. 5a, in the current range of 0.5–2 A g^{-1}, the specific capacity of the $LiCr_{0.05}Fe_{0.05}Mn_{1.9}O_4$ electrode is close to that of the pristine $LiMn_2O_4$ electrode at any current rate, but that of the $LiCr_{0.1}Fe_{0.1}Mn_{1.8}O_4$ electrode is obviously decreased. When the current is increased from 0.5 to 2 A g^{-1}, the specific capacities of the $LiMn_2O_4$, $LiCr_{0.05}Fe_{0.05}Mn_{1.9}O_4$ and $LiCr_{0.1}Fe_{0.1}Mn_{1.8}O_4$ electrodes are decreased from 121, 120, and 111 to 90, 90, and 81 mAh g^{-1}, respectively, i.e., decreased by 26%, 25%, and 27%, respectively, suggesting good high-rate capability.

Two potential plateaus can be observed in the discharge curves (Fig. 5b) which correspond to the two reduction waves in the CVs in Fig. 3. The first discharge plateaus for the doped $LiCr_xFe_xMn_{2-2x}O_4$ electrodes are obviously

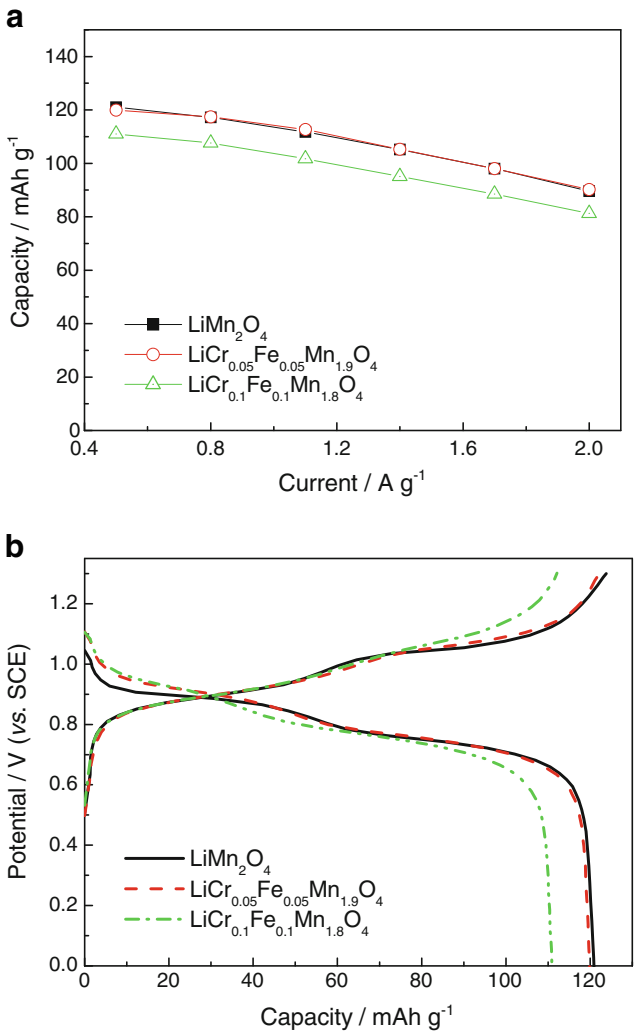

Fig. 5 Discharge-specific capacities of the $LiCr_xFe_xMn_{2-2x}O_4$ (x=0, 0.05, 0.1) electrodes at different charge/discharge current rates (**a**) and charge/discharge curves at the current rate of 0.5 A g^{-1} (**b**)

higher than that of the pristine $LiMn_2O_4$ electrode. Two charge plateaus could be observed for the pristine $LiMn_2O_4$ and the $LiCr_{0.05}Fe_{0.05}Mn_{1.9}O_4$ electrodes. However, the two charge plateaus for the $LiCr_{0.1}Fe_{0.1}Mn_{1.8}O_4$ electrode are inconspicuous. These charge/discharge characteristics are, on the whole, consistent with the CVs in Fig. 3. At the current rate of 0.5 A g^{-1}, the discharge-specific capacity of the $LiCr_{0.05}Fe_{0.05}Mn_{1.9}O_4$ electrode is only a little lower than that of the pristine $LiMn_2O_4$ electrode. However, the discharge-specific capacity of the $LiCr_{0.1}Fe_{0.1}Mn_{1.8}O_4$ electrode is obviously lower than that of the pristine $LiMn_2O_4$ electrode.

The cycle performances of the $LiMn_2O_4$, $LiCr_{0.05}Fe_{0.05}Mn_{1.9}O_4$, and $LiCr_{0.1}Fe_{0.1}Mn_{1.8}O_4$ electrodes are presented in Fig. 6. The electrodes are cycled over the operating potential range of 0 to 1.3 V (SCE) at a high charge/discharge current rate of 2 A g^{-1}. As can be seen,

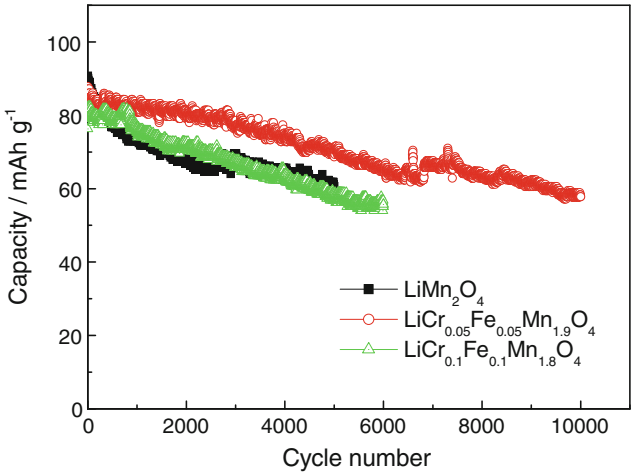

Fig. 6 Cycle performances of $LiCr_xFe_xMn_{2-2x}O_4$ (x=0, 0.05, 0.1) electrodes at a high current rate of 2 A g^{-1}

the capacity of the pristine $LiMn_2O_4$ electrode degrades fast, especially in the initial 2,000 cycles. After 5,000 cycles, 69% of the initial capacity is maintained. The initial specific capacity of the $LiCr_{0.05}Fe_{0.05}Mn_{1.9}O_4$ electrode is close to that of the pristine $LiMn_2O_4$ electrode, but its cycling stability is obviously prior to that of the pristine $LiMn_2O_4$ electrode. After 9,000 cycles, 71% of the initial capacity is maintained; after 10,000 cycles, 67% of the initial capacity is maintained. Meanwhile, the initial specific capacity of the $LiCr_{0.1}Fe_{0.1}Mn_{1.8}O_4$ electrode is obviously lower than that of the former electrodes. After 6,000 cycles, the capacity retention is 70%.

Theoretically, cation (lower than tetravalent) substitution for Mn^{3+} in $LiMn_2O_4$ can reduce the specific capacity of the spinel at the 4-V (vs. Li^+) level, and the decrement will increase with increasing the doping amount. On the other hand, Jahn–Teller effect could be depressed to a certain degree due to the reduction of Mn^{3+} ions in the spinel, and subsequently the cycling stability of the spinel would be improved. In nonaqueous electrolytes, Cr [15, 30] or Fe [16, 28], etc., partial substitution for Mn indeed decreased the specific capacity of $LiMn_2O_4$ at the 4-V level, but it improved the cycling stability.

Conclusions

$LiCr_xFe_xMn_{2-2x}O_4$ (x=0, 0.05, 0.1) electrode materials were prepared by sol–gel method. XRD analysis revealed that the doped $LiCr_xFe_xMn_{2-2x}O_4$ materials are phase-pure spinels. The electrochemical performances of the $LiMn_2O_4$, $LiCr_{0.05}Fe_{0.05}Mn_{1.9}O_4$, and $LiCr_{0.1}Fe_{0.1}Mn_{1.8}O_4$ electrodes in 5 M $LiNO_3$ aqueous electrolyte were studied with

comparison. The experimental results demonstrated that the specific capacity of the $LiCr_{0.05}Fe_{0.05}Mn_{1.9}O_4$ electrode is close to that of the $LiMn_2O_4$ electrode in the current range of 0.5–2 A g^{-1}, but the specific capacity of the $LiCr_{0.1}Fe_{0.1}Mn_{1.8}O_4$ electrode is obviously lower than that of the $LiMn_2O_4$ electrode. The initial specific capacity of the $LiCr_{0.05}Fe_{0.05}Mn_{1.9}O_4$ electrode is close to that of the pristine $LiMn_2O_4$ electrode at the high current rate of 2 A g^{-1}, but its charge/discharge cyclability is obviously prior to that of the pristine $LiMn_2O_4$ electrode.

Acknowledgments This work was supported by Leading Academic Discipline Project of Shanghai Municipal Education Commission (project number: J50102). Center of Instrumental Analysis and Test of Shanghai University is gratefully acknowledged for XRD, TEM, and HRTEM experiments.

References

1. Li W, Dahn JR, Wainwright DS (1994) Science 264:1115–1118
2. Wang GX, Zhong S, Bradhurst DH, Dou SX, Liu HK (1998) J Power Sources 74:198–201
3. Li NC, Patrissi CJ, Che GL, Martin CR (2000) J Electrochem Soc 147:2044–2049
4. Eftekhari A (2001) Electrochim Acta 47:495–499
5. Jayalakshmi M, Mohan Rao M, Scholz F (2003) Langmuir 19:8403–8408
6. Lee JW, Pyun SI (2004) Electrochim Acta 49:753–756
7. Nakayama N, Nozawa T, Iriyama Y, Abe T, Ogumi Z, Kikuchi K (2007) J Power Sources 174:695–700
8. Cvjeticanin N, Stojkovic I, Mitric M, Mentus S (2007) J Power Sources 174:1117–1120
9. Tonti D, Torralvo MJ, Enciso E, Sobrados I, Sanz J (2008) Chem Mater 20:4783–4790
10. Katakura K, Wada K, Kajiki Y, Yamamoto A, Ogumi Z (2009) J Power Sources 189:240–247
11. Tian L, Yuan AB (2009) J Power Sources 192:693–697
12. Nieto S, Majumder SB, Katiyar RS (2004) J Power Sources 136:88–98
13. Kakuda T, Uematsu K, Toda K, Sato M (2007) J Power Sources 167:499–503
14. Liu RS, Shen CH (2003) Solid State Ionics 157:95–100
15. Thirunakaran R, Kim KT, Kang YM, Seo CY, Young-Lee J (2004) J Power Sources 137:100–104
16. Kim BH, Choi YK, Choa YH (2003) Solid State Ionics 158:281–285
17. Wang XQ, Tanaike O, Kodama M, Hatori H (2007) J Power Sources 168:282–287
18. Shaju KM, Subba Rao GV, Chowdari BVR (2002) Solid State Ionics 148:343–350
19. Sakunthala A, Reddy MV, Selvasekarapandian S, Chowdari BVR, Selvin PC (2010) Electrochim Acta 55:4441–4450
20. Fey GTK, Lu CZ, Kumar TP (2003) Mater Chem Phys 80:309–318
21. Hwang BJ, Tsai YW, Santhanam R, Hu SK, Sheu HS (2003) J Power Sources 119–121:727–732
22. Stojkovic IB, Cvjeticanin ND, Mentus SV (2010) Electrochem Commun 12:371–373
23. Yuan AB, Tian L, Xu WM, Wang YQ (2010) J Power Sources 195:5032–5038
24. Wang HC, Lu CH (2003) J Power Sources 119–121:738–742
25. Mateyshina YG, Lafont U, Uvarov NF, Kelder EM (2008) Solid State Ionics 179:192–196
26. Ohzuku T, Ariyoshi K, Takeda S, Sakai Y (2001) Electrochim Acta 46:2327–2336
27. Zeng RH, Li WS, Lu DS, Huang QM (2007) J Power Sources 174:592–597
28. Bang HJ, Donepudi VS, Prakash J (2002) Electrochim Acta 48:443–451
29. Shi SQ, Ouyang CY, Wang DS, Chen LQ, Huang XJ (2003) Solid State Commun 126:531–534
30. Suryakala K, Kalaignan GP, Vasudevan T (2007) Mater Chem Phys 104:479–482